International Journal of Advances in Electrical Engineering

E-ISSN: 2708-4582
P-ISSN: 2708-4574
IJAEE 2021; 2(1): 19-31

www.electricaltechjournal.com
Received: 14-11-2020
Accepted: 19-12-2020

Ogunwuyi OJ
Department of Electrical and Electronic Engineering, Faculty of Engineering, Osun, Polytechnic, Iree, Nigeria

Bisiriyu AO
Department of Electrical and Electronic Engineering, Faculty of Engineering, Osun, Polytechnic, Iree, Nigeria

Ajetunmobi EO
Department of Electrical and Electronic Engineering, Faculty of Engineering, Osun, Polytechnic, Iree, Nigeria

Omotayo ME
Department of Electrical and Electronic Engineering, Faculty of Engineering, Osun, Polytechnic, Iree, Nigeria

Correspondence
Ogunwuyi OJ
Department of Electrical and Electronic Engineering, Faculty of Engineering, Osun, Polytechnic, Iree, Nigeria

Development of predictive control of a permanent-magnet synchronous motor for improvement of steady state response

Ogunwuyi OJ, Bisiriyu AO, Ajetunmobi EO and Omotayo ME

Abstract
The traditional model predictive current control (MPCC) strategy has the advantages of a fast dynamic response and flexible constraint conditions. However, this strategy only determines the optimal voltage vector in a period rather than in multiple periods, which may result in a large current ripple. To solve the above problem, this paper proposes a multi-step MPCC strategy of permanent-magnet synchronous motor. In the proposed multi-step MPCC strategy, the optimal voltage vector and the sub-optimal voltage vector are considered simultaneously. The current response in the next period is predicted on the basis of the optimal and the sub-optimal voltage vectors, respectively. To ensure the optimality of the selected voltage vector in two control periods, the current responses of the two control periods are contrasted. Compared with the traditional MPCC strategy, simulation and experimental results show that the proposed multi-step MPCC strategy can effectively reduce the current ripple and improve the steady-state performance without increasing the switching frequency.

Keywords: Permanent-magnet synchronous motor • Multi-step model predictive control • Current ripple

1. Introduction
The SPMSM has quick response, high power density, and high efficiency. It has become increasingly popular as the cost of rare-earth materials has decreased and their performance has improved [1]. SPMSM control strategies have thus become a research hotspot. Vector control is a classic SPMSM control strategy. This strategy has good steady-state performance but needs to improve dynamic performance [2].
In addition to vector control, model predictive control (MPC) is a common type of control strategy for SPMSM. Fast dynamic response and easy inclusion of multiple objectives are advantages of MPC [3]. MPC strategy is divided into two parts: CCS-MPC and FCS-MPC, depending on whether pulse width modulation is required [4]. Online optimization solves CCS-MPC's voltage reference problem. Low current ripple and high accuracy in steady-state. But it has a high switching frequency and high switching losses. The FCS-MPC fully considers the discrete characteristic of inverter, and has the advantages of a simple control concept and easy implementation.
FCS-MPC is based on a finite number of voltage vectors. To predict the next control period's controlled quantity, use a mathematical model. The inverter then uses the voltage vector that brings the predictive value closest to the reference [5]. Due to FCS-limited MPC's control set, steady-state performance must be improved. The prediction horizon [6], the candidate number of vectors [7], prediction error correction [8] and delay compensation [9] have all been proposed to improve FCS-MPC steady-state performance.
Model predictive current control (MPCC) has a large current ripple, since the selected voltage vector amplitude and direction are fixed. A method of increasing the candidate vector number is proposed for the above problem [10]. Proposed a two-vector MPCC strategy for this method. A three-vector MPCC strategy was also proposed based on the two-vector strategy in [11]. Increasing the number of vectors reduces the current ripple. However, in [10] and [11], this method raises the switching frequency. When the parameters of the control object are changed during the operation process, the prediction algorithm of the MPCC strategy is inaccurate due to parameter mismatch. In a method for prediction error correction, the prediction error term is added to the predictive mathematical model for reducing the impact of parameter change [12, 13].

In MPCC, there are inevitably a sampling delay and a calculation delay in the actual operation of the system. Therefore, delay compensation is used to improve the steady-state performance [14, 15].

1.1 Discrete mathematical model of the SPMSM

The mathematical model of a surface mount SPMSM (d-q reference frame) is as follows:

$$\frac{di_q}{dt} = \frac{1}{L_s}\left[u_q - R_s i_q - \omega_{re} L_s i_d - \omega_{re}\psi_f\right] \quad (1)$$

$$\frac{di_q}{dt} = \frac{1}{L_s}\left[u_q - R_s i_q - \omega_{re} L_s i_d\right] \quad (2)$$

$$T_e = \frac{3}{2} p\psi_f i_q, \quad (3)$$

Where L_s is the stator inductance, and R_s is the stator resistance. ®re is the rotor electrical angular velocity, i^f is the permanent-magnet flux, u_d and u_q are the d-axis and q-axis voltages, i_d and i_q are the d-axis and q-axis currents, T_e is the electromagnetic torque, and p is the number of pole pairs.
Equations (1) and (2) can be obtained using first-order Euler discretization as follows:

$$i_d(k+1) = i_d(k) + \frac{T_s}{L_s}\left[u_d(k) - R_s i_d(k) + E_d(k)\right] \quad (4)$$

$$i_q(k+1) = i_q(k) + \frac{T_s}{L_s}\left[u_q(k) - R_s i_q(k) + E_q(k)\right] \quad (5)$$

$$E_q(k) = -\omega_{re}(k) L_s i_d(k) - \omega_{re}(k)\psi_f \quad (6)$$

$$E_d(k) = \omega_{re}(k) L_s i_q(k) \quad (7)$$

where $E_d(k)$ and $E_q(k)$ are the back electromotive forces of the d-axis and q-axis at the kth instant, u_d and u_q are the d-axis and q-axis voltages at the kth instant, i_d (k) and $i_q(k)$ are the currents of the d-axis and q-axis at the kth instant, T_s is the control period, and $i_d(k+1)$ and $i_q(k+1)$ are the d-axis and q-axis predictive currents at the (k + 1)th instant.

1.2 Traditional MPCC strategy analysis

Unavoidable calculation delay as a result, the optimal voltage vector selected for the SPMSM is used for the next control period, resulting in system control performance degradation. Thus, the one-step calculation delay must be compensated. It can be updated as:

$$i_d(k+2) = i_d(k+1) + \frac{T_s}{L_s}\left[u_d(k+1) - R_s i_d(k+1) + E_d(k+1)\right] \quad (8)$$

$$i_q(k+2) = i_q(k+1) + \frac{T_s}{L_s}\left[u_q(k+1) - R_s i_q(k+1) + E_q(k+1)\right] \quad (9)$$

Where $i_d(k+1)$ and $i_q(k+1)$ are the compensated currents. $i_d(k+2)$ and $i_q(k+2)$ are the predictive currents at the (k + 2) the instant.
A two-level three-phase voltage source inverter has six nonzero voltage vectors and two zero vectors. So there are seven types of voltage vectors. Using Eqs. (8) and (9), predict currents for various voltage vectors. The classic MPCC technique determines the best voltage vector that minimizes the cost function while maximizing the predictive current. The cost function is:

$$g_i = \left|i_q^* - i_q(k+2)\right| + \left|i_d^* - i_d(k+2)\right| \quad (10)$$

Where i^* is the d-axis current reference, and i^* is the q-axis current reference.
For the d-axis and q-axis currents, the principle for selecting the optimal voltage vector is the same. Therefore, the process of selecting optimal voltage vector by the *q*-axis current is taken as an example. Figure 1 shows a diagram of the process for selecting optimal voltage vector in the traditional MPCC strategy. In Fig. 1, $i_q(k+1)$ is calculated by delay compensation. The current value $i_q\backslash_i(k+2)$ (*i* e 0,1..., 6) can be predicted separately under the actions of seven voltage vectors. The voltage vector that corresponds to the current minimum error is chosen to act on the system. In Fig. 1, $i_q\backslash_2(k+2)$ is closest to the reference current. Thus, V_2 is the optimal voltage vector.
Traditionally, MPCC only confirms the best voltage vector in one control period. The standard MPCC technique ignores the optimization of the adjacent control period. Thus, the selected vector in each control period is optimal for the current period. A significant current ripple may ensue. We now have proof that extending the forecasting horizon can lower the present swell A multi-step MPCC technique to reduce current ripple without increasing switching frequency is proposed here.

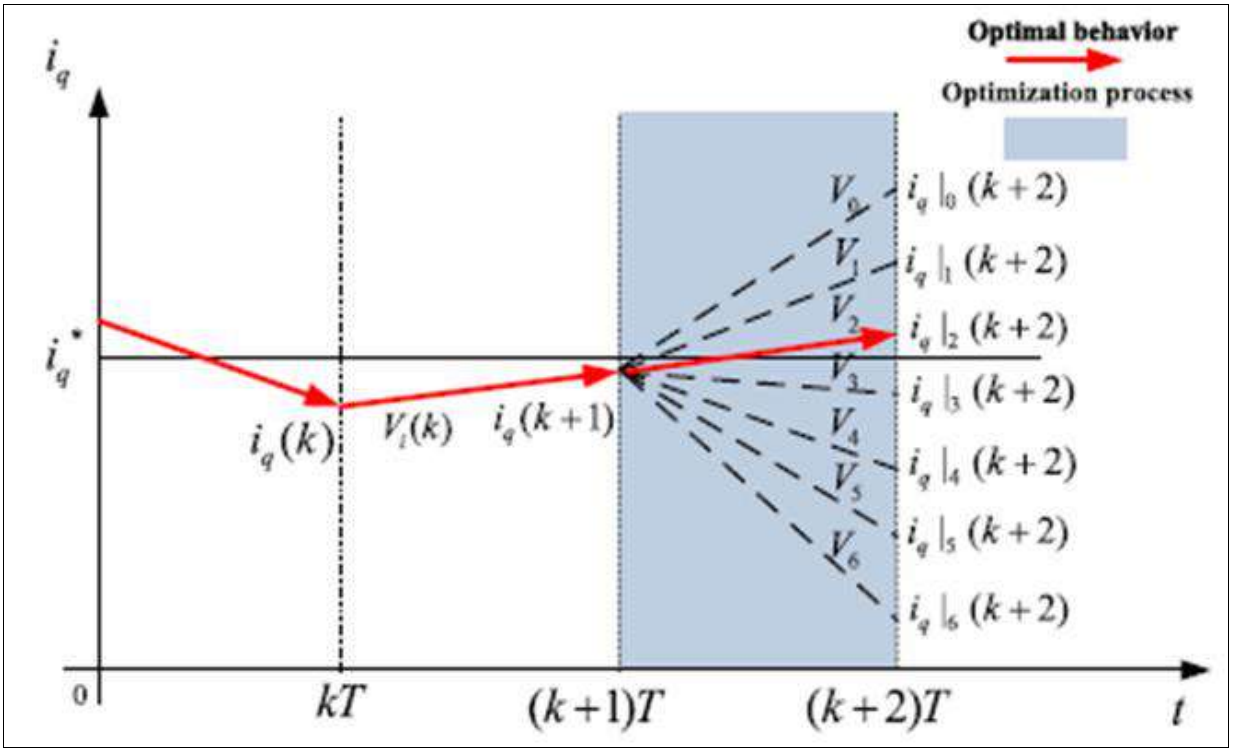

Fig 1: Diagram of the process for selecting optimal voltage vector in the traditional MPCC strategy.

2. Material and Method

2.1 Multi-step MPCC method analysis

In the traditional MPCC strategy, the mathematical model of the control object becomes

$$x(k+1) = A^2 x(k) + Bu(k) \tag{11}$$

$$x(k+N) = A^N x(k) + A^{N-1} Bu(k) + \cdots + Bu(k+N-1)$$

So, the predictive value at (k+A) is determined by all selected voltage vectors from k to (k + A-1). Optimal information from all voltage vectors should be assessed simultaneously to confirm optimality in various periods.

The typical MPCC technique is conservative since it does not consider future voltage vectors. So the prediction horizon must be extended. In this case, the proposed cost function is:

$$J_N = \sum_{l=k}^{k+N-1} \left\| i_d(l+1) - i_d^* \right\|_2^2 + - \left\| i_q(l+1) - i_q^* \right\|_2^2 \tag{14}$$

It is possible to substitute all alternative voltage vectors into the cost function (14), and then find the least one. The ideal voltage is the cost function's minimal value.

Vector. However, a comprehensive optimization strategy necessitates substantial processing power [23]. If N = 3, the 2L-VSI calculates the cost function 399 times. This study considers controller computation. So the prediction horizon is two steps and some voltage vectors with severe current errors are discarded.

The predictive value in two predictive periods is given by

$$x(k+2) = A^2 x(k) + ABu(k) + Bu(k+1) \tag{12}$$

The predictive value in N control periods can be obtained by

(13)

2.2 Optimal voltage vector selecting process in the multi - step MPCC strategy

The multi-step MPCC approach selects the applied voltage vector as follows. Eqs. (8) And (9) determine the predicted current for seven basic voltage vectors (9). The predicted current closest to the reference is id min1 (k + 2) and iqmin1 (k + 2). The optimal voltage vector is Vmin1. The second closest predictive current is expressed as idmin2 (k + 2) and iqmin2 (k + 2). Identically, the sub-optimal voltage vector is written as V min 2.

The proposed multi-step MPCC technique is shown in Figure 2. Delay compensation calculates iq(k + 1). The optimal voltage vector Vmin1 and the sub-optimal voltage vector Vmin2 are chosen. The selection of candidate voltage vectors took into account current errors at (k + 2)T. The proposed technique predicts the current value under the seven voltage vector actions using the current response under Vmin1, and minCost1 is the current prediction error at (k + 3)T. The current values are predicted for the seven voltage vector operations at the same time using the current response of Vmin2, and minCost2 is the current prediction error at (k + 3)T. In Fig. 2,

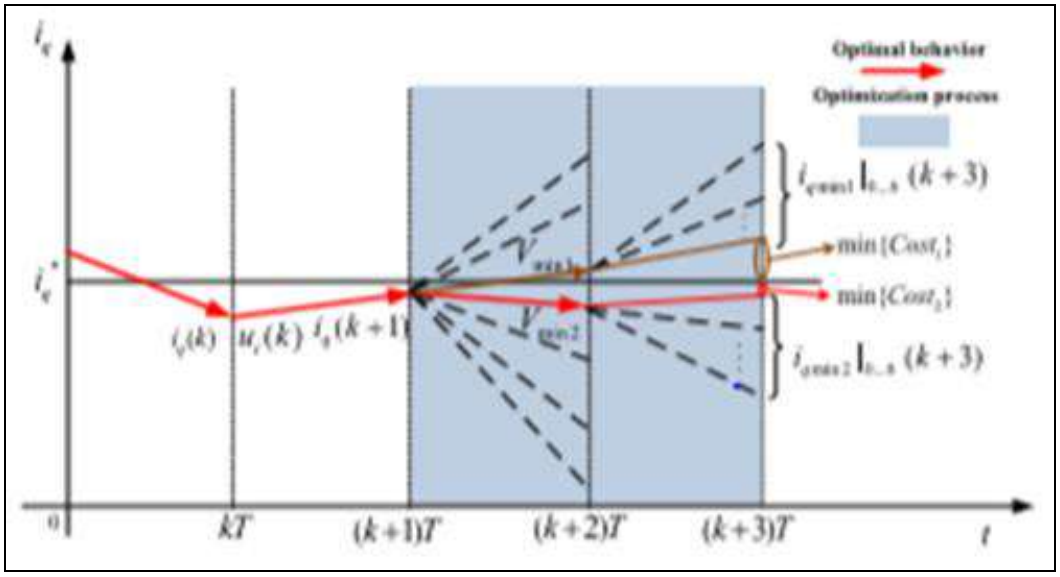

Fig 2: Voltage vector action diagram of the multi-step MPCC strategy

Acted on the system at (k + 1) T since min {$Cost_2$} is smaller than min{$Cost_1$}.
The concrete process performs the following step.

Equations (15) and (16) can calculate the predictive current of the next period based on V_{min1} (k + 1) using i_{dmin1}(k + 2) and i_{qmin1}(k + 2):

$$i_{d\min 1}(k+3) = i_{q\min 1}(k+2) + \frac{T_s}{L_s}\left[u_q(k+2) - R_s\, i_{d\min}(k+2) + E_q(k+2)\right] \quad (15)$$

$$i_{q\min 1}(k+3) = i_{q\min 1}(k+2) + \frac{T_s}{L_s}\left[u_q(k+2) - R_s\, i_{d\min}(k+2) + E_q(k+2)\right] \quad (16)$$

Where $i_{d\min 1}(k+3)$ and $i_{q\min 1}(k+3)$ are predictive currents at (k + 3) T on the basis of V_{min1} (k + 1). Then, the seven sets of predictive current values under the action of all the voltage vectors are substituted into Eq. (17). The purpose is to find the minimum value of $Cost_1$. Equation (17) is given by

$$Cost_2 = \left|i_q^* - i_{q\min 2}(k+3)\right| + \left|i_q^* - i_{q\min 2}(k+3)\right|. \quad (17)$$

To obtain the predictive current at the next period based on V_{min2} (k + 1), Eqs. (18) And (19) can be given by

$$i_{d\min 2}(k+3) = i_{d\min 2}(k+2) + \frac{T_s}{L_s}\left[u_d(k+2) - R_s\, i_{d\min 2}(k+2) + E_d(k+2)\right] \quad (18)$$

$$i_{q\min 2}(k+3) = i_{q\min 2}(k+2) + \frac{T_s}{L_s}\left[u_q(k+2) - R_s\, i_{q\min 2}(k+2) + E_q(k+2)\right] \quad (19)$$

Where i_{dmin2} (k + 3) and i_{qmin2} (k + 3) are predictive currents at (k + 3)T on the basis of V_{min2}(k + 1).
i_{dmin2} (k + 3) and i_{qmin2} (k + 3) are predicted on the basis of the seven voltage vectors. The seven sets of predictive current values are substituted into Eq. (20) to obtain the minimum value of $Cost_2$. The equation is shown as

$$Cost_2 = \left|i_q^* - i_{q\min 2}(k+3)\right| + \left|i_d^* - i_{d\min 2}(k+3)\right|. \quad (20)$$

To determine the voltage vector to apply to the inverter, Eq (21). The equation is:

$$V_{out} = \begin{cases} V_{\min 1,} & \min\{Cost_1\} \le \min\{Cost_2\} \\ V_{\min 2,} & \min\{Cost_1\} > \min\{Cost_2\} \end{cases}. \quad (21)$$

The multi-step MPCC technique enables excellent voltage vector selection for two control periods. During the two control periods, the multi-step MPCC method tracks the current reference better. Fig. 3 depicts a flow chart of the multi-step MPCC strategy voltage vector selection.

2.3 Multi- step MPCC strategy

Figure 4 depicts the multi-step MPCC method. The multi-step MPCC strategy's object is SPMSM. Coordinate transformation, delay compensation, and multi-step model predictive current controller comprise its core. A maximum torque per ampere control for the SPMSM is shown in Fig. 4. Figure 5 depicts a multi-step model predictive current controller. Clearly, the suggested multi-step MPCC technique borrows heavily from the classic MPCC strategy. Thoughts on how to select the appropriate voltage vector.

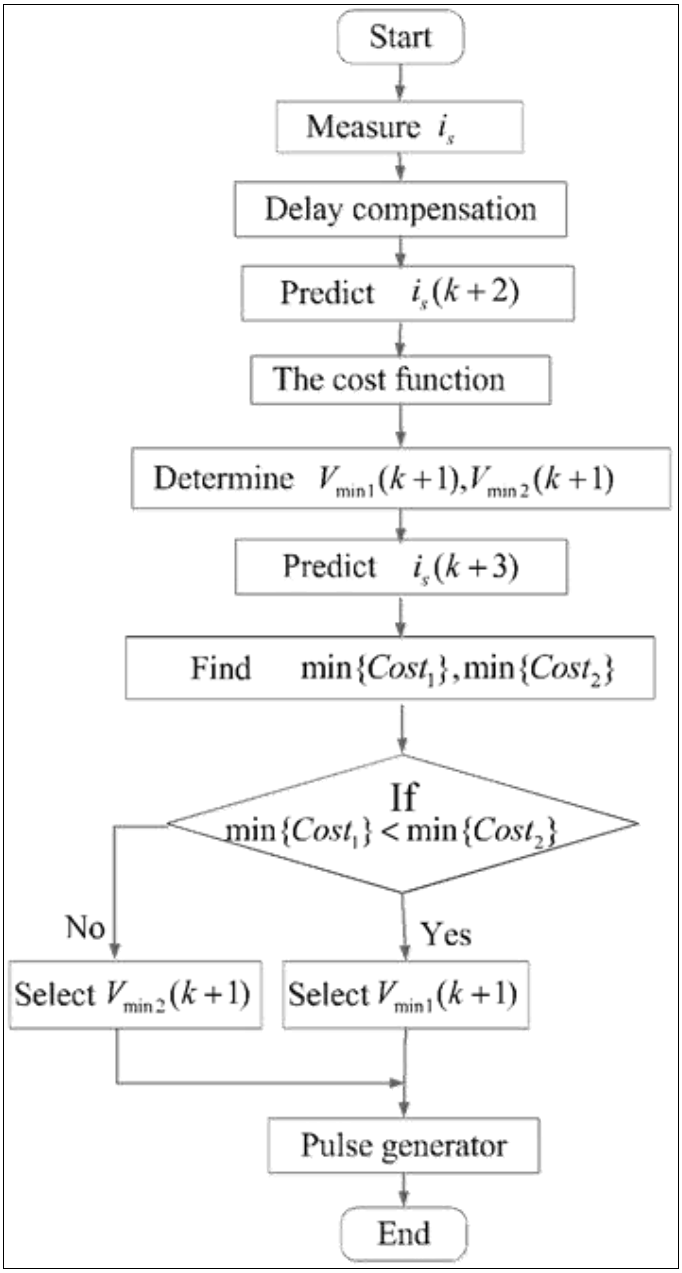

Fig 3: Flow chart of the multi-step MPCC strategy voltage vector selection

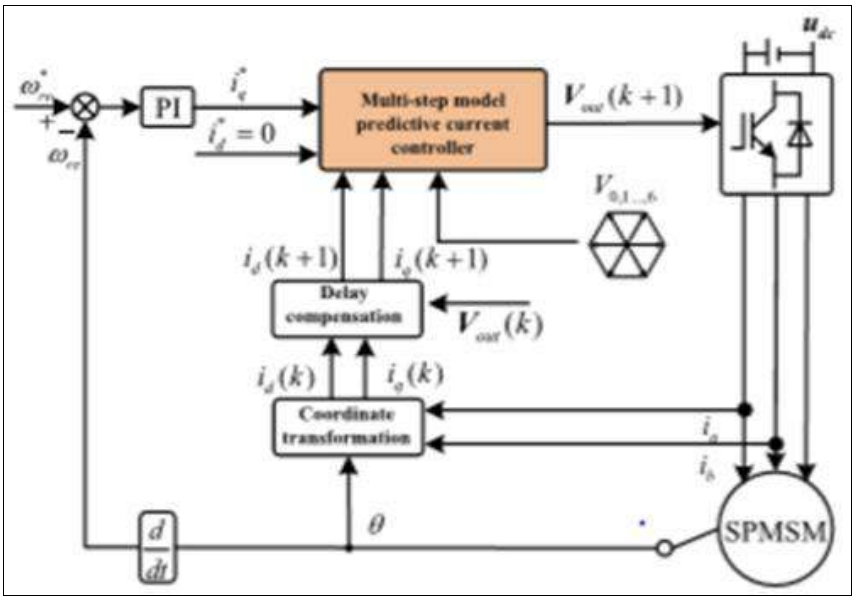

Fig 4: Block diagram of the proposed multi-step MPCC strategy

In the classic MPCC technique, the ideal voltage vector is selected in one step. The multi-step MPCC technique examines both the optimal and sub-optimal voltage vectors. In two control periods, the predictive current of the chosen voltage vector action is closer to the reference than the conventional method. Because the multi-step MPCC technique applies a voltage vector in one control period, the switching frequency is identical. Compared to the typical MPCC method, the proposed strategy's steady-state performance can be enhanced. Figure 6 depicts the 2L-VSI voltage vector set. One voltage vector equals one switching sequence in the 2L-VSI. Theoretically, traditional MPCC and multi-step MPCC use only one voltage vector every control period. So both strategies have a comparable switching frequency over time. Each control's specified voltage vector

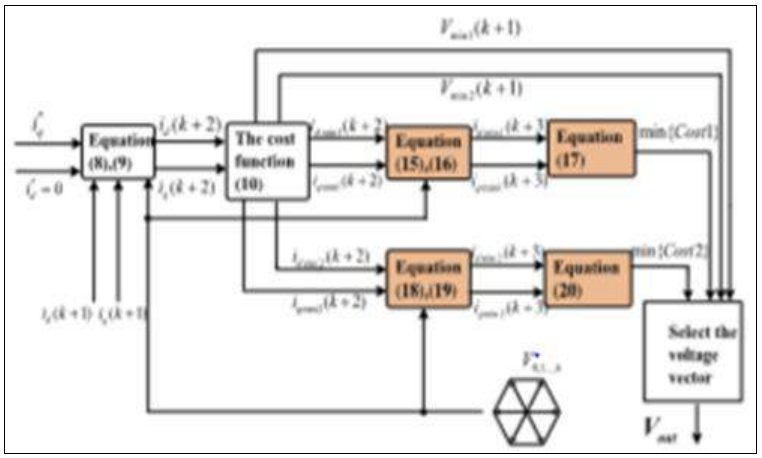

Fig 5: Block diagram of the proposed multi-step model predictive current controller

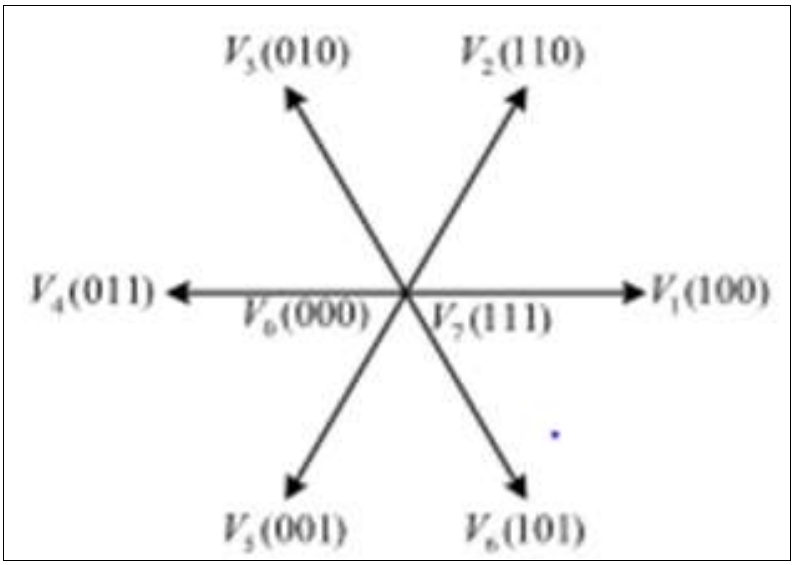

Fig 6: Finite voltage vector set of a 2L-VSI

MPCC and multi-step MPCC techniques have no defined time. So the switching frequency varies. The average switching frequency of the two techniques is calculated as in [23] by adding up all the switches over a period of time. The switching frequency fav equation is:

$$f_{av} = N / 6 / \Delta t \quad (22)$$

Where N is the number of switches accumulated during ΔT

3. Result and Discussion

The simulation and experimental results of the classic MPCC and multi-step MPCC techniques are compared to demonstrate their practicality. Both strategies use 10 kHz sampling. Both algorithms employ the same SPMSM and speed PI parameters. The SPMSM parameters are listed in Table 1.

3.1 Simulation results

Figures 7, 8 and 9 illustrate simulation results for classic MPCC and multi-step MPCC techniques. Starting, changing speed, and changing load torque are all simulated in Figure 7.

Table 1: Parameters of the SPMS

Motor parameters	Values
Rotor flux linkage/Wb	0.253
Stator inductance/mH	21.73
Rated voltage/V	382
Rated current/A	4.4
Stator resistance/Ω	2.725
Rated speed/(r/min)	2430
Number of pole pairs	4
Rotor inertia/(kg cm^2)	12
Rated torque/(N m)	9.6

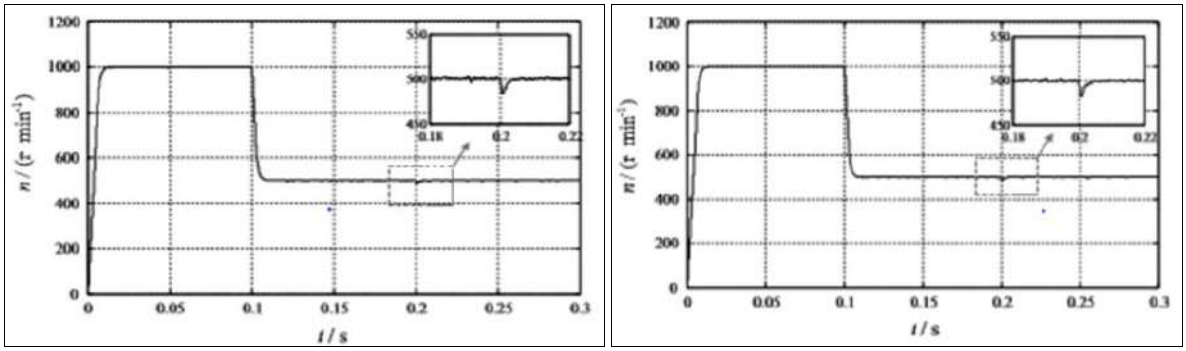

(a) (b)

Fig 7: Simulation results under speed and load changes: a traditional MPCC; b multi-step MPCC

Traditional MPCC vs. proposed multi-step MPCC The initial reference speed is 1000r/min and then drops to 500r/min in 0.1 s. In 0.2 s, the load torque goes from zero to 50% of the rated load. Contrary to popular belief, the proposed multi-step method can adapt to variations in both speed and load. Figure 8 displays the two techniques' steady-state performance waveforms at 1000rpm with the rated load. Its present THD is 8.01 percent, while the planned multi-step MPCC strategy's is 5.96 percent. The proposed technique outperforms the classic MPCC strategy in steady state. Fig. 9 shows the outcomes of the two procedures at different speeds to compare the switching frequencies. Also, the suggested multi-step MPCC method has almost the same switching frequency as the classic MPCC approach, proving the compatibility of simulation and theoretical analysis results.

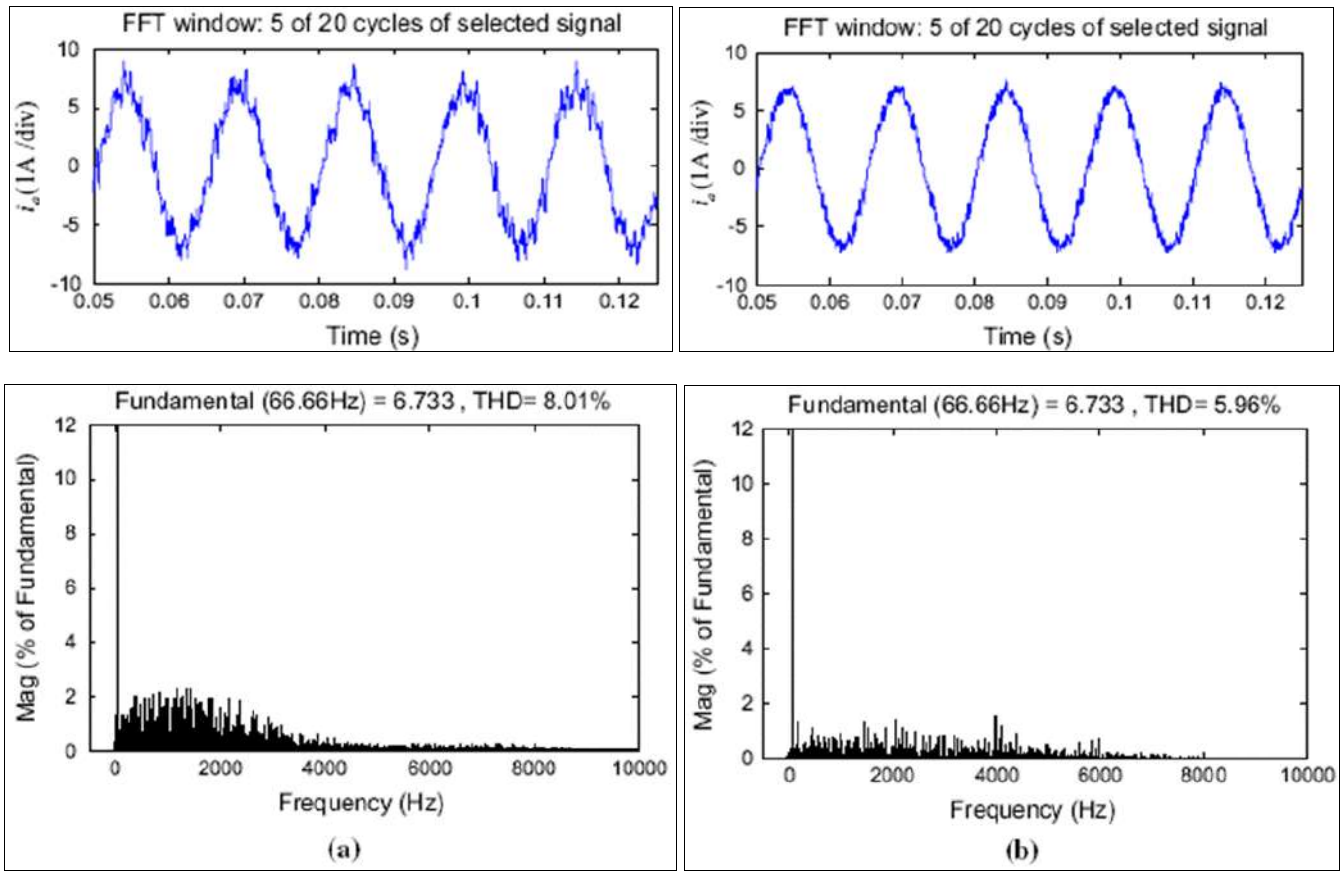

Fig 8: Steady-state performance simulation results of the: a traditional MPCC; b multi-step MPCC

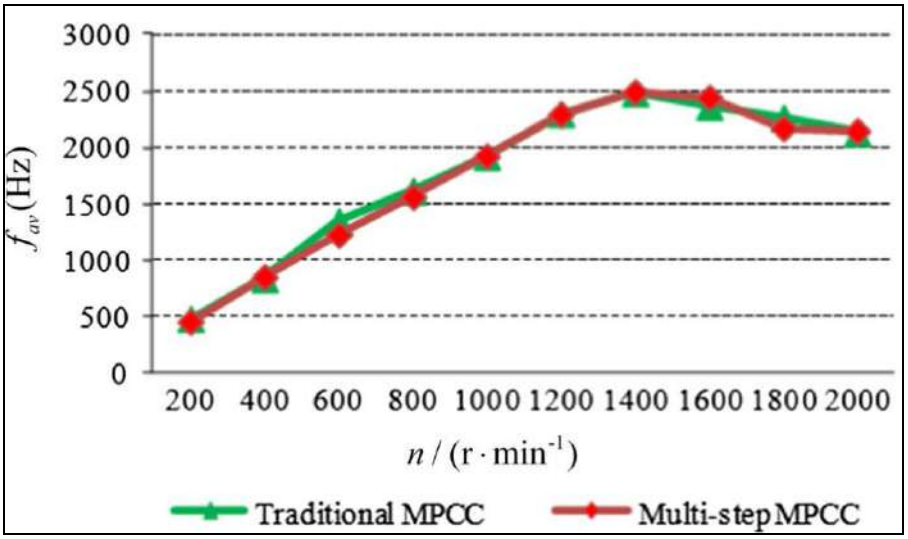

Fig 9: Switching frequency simulation results of the traditional MPCC and the multi-step MPCC

3.2 Dynamic performance of experimental results

Figure 10 displays the experimental setup. Parts include the control board, voltage source inverter, load motor, and SPMSM. The control board and voltage source inverter are run by My Way's Expret3 system. A TMS320C6713 DSP with a SPARTAN-XC3S1500 FPGA. The drag system has a load motor and an SPMSM.

Figure 11 displays the classic MPCC and the proposed multi-step MPCC techniques' beginning and speed reversal waveforms. Initial speed is 1000r/min. At 0.56 s, the reference speed changes to 500r/min. As shown, the multi-step MPCC technique is as quick as the traditional MPCC strategy.

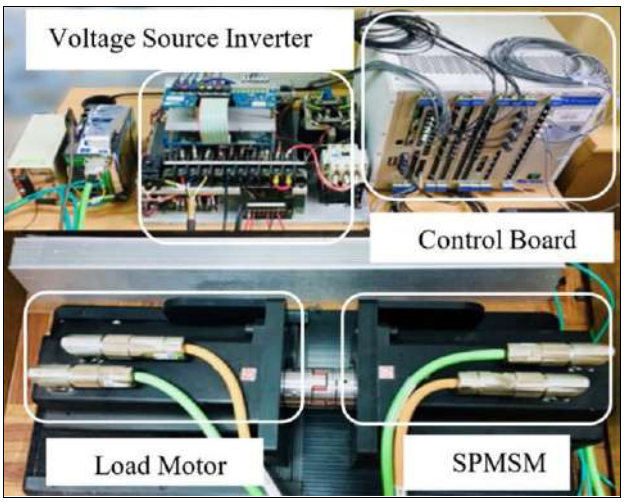

Fig 10: Diagram of the experimental equipment

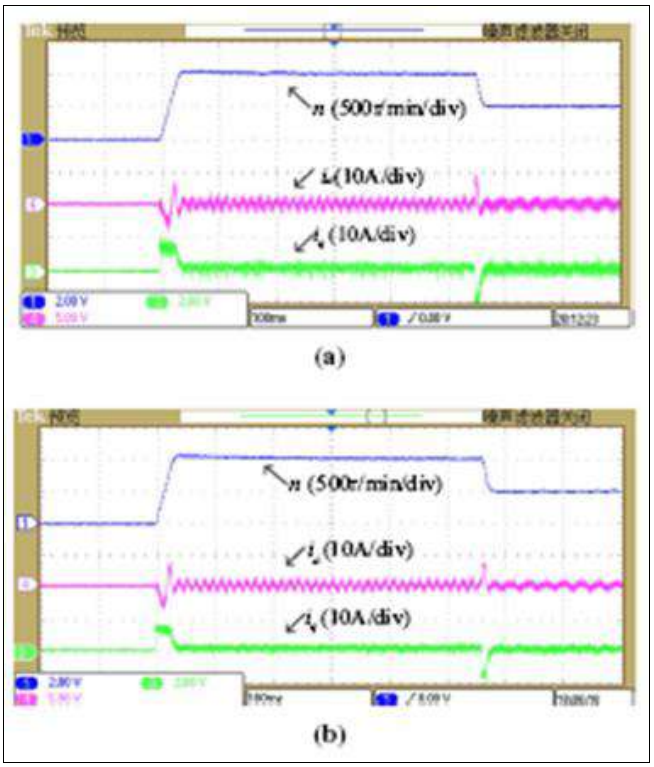

Fig 11: Experimental results at startup: a traditional MPCC; b multi-step MPCC

As shown in Figure 12, the standard MPCC and multi-step MPCC techniques use SPMSM speed and current waveforms from 100% rated load to 0%. 12) The multi-step technique follows the load change as quickly as the classic strategy.

3.3 Steady‐state performance of experimental results

Figure 13 shows i_q and i_d experimental waveforms of the traditional MPCC and the multi-step MPCC strategies at 500r/min and no load. To further analyze the current ripple, 125,016 sets of experimental data are obtained from the oscilloscope. The current ripple is calculated by the standard deviation equation in [24]. The standard deviation equation is given by:

$$\Delta i_d = \sqrt{\frac{1}{N}\sum_{n=1}^{N}\left(i_d(n) - i_{d\_ave}\right)^2} \quad (23)$$

$$\Delta i_q = \sqrt{\frac{1}{N}\sum_{n=1}^{N}\left(i_q(n) - i_{q\_ave}\right)^2} \quad (24)$$

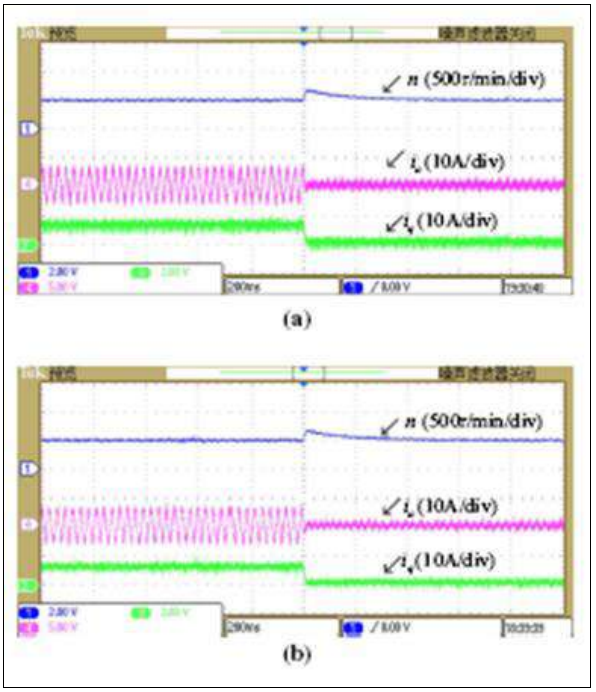

Fig 12: Experimental results at a changed torque: a traditional MPCC; b multi-step MPCC

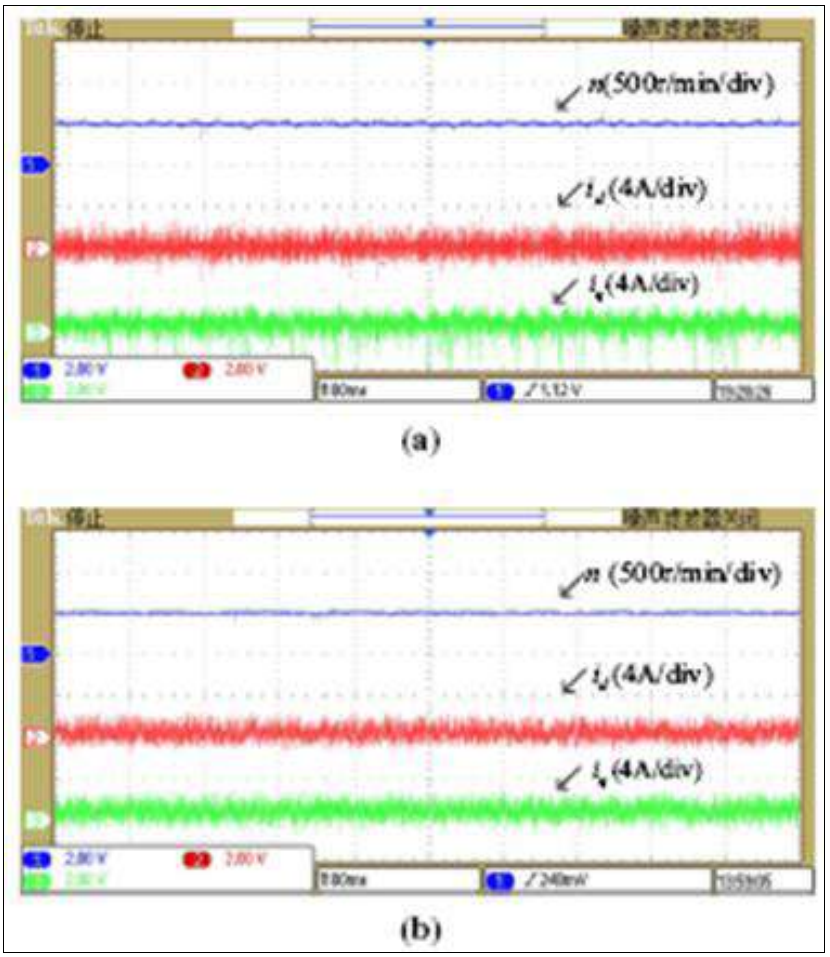

Fig 13: Experimental results at 500r/min without a load: a traditional MPCC; b multi-step MPCC

Table 2: Current ripple of two control strategies at 500r/min without a load

Strategy	Δi_d(A)	Δi_q(A)
The traditional MPCC	1.42	1.39
The multi-step MPCC	1.04	0.96
Reduced percentage (%)	26.7	30.4

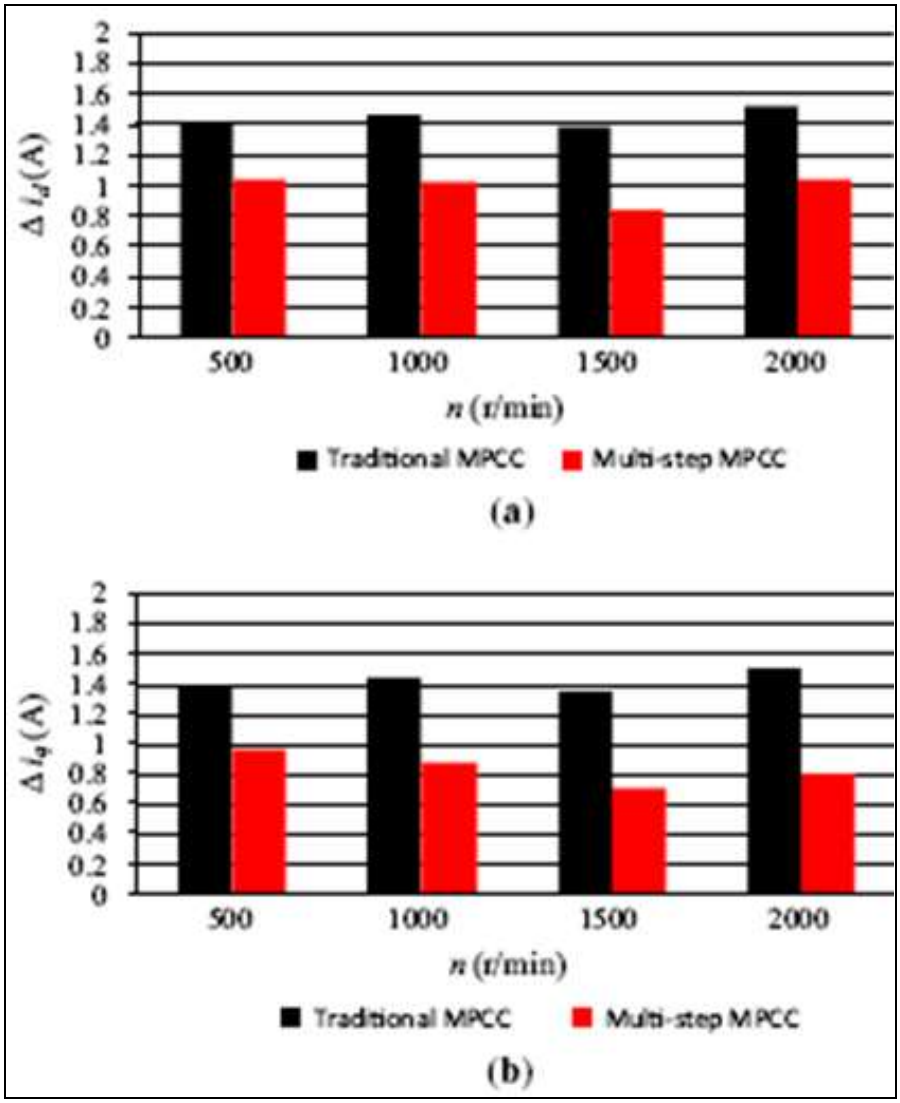

Fig 14: Experimental current ripple of the traditional MPCC and the multi-step MPCC at different speeds without a load: a *d*-axis current ripple; b *q*-axis current ripple

Id ave and Iq ave are the average currents of the d- axis and q-axis, respectively. (2) shows the present ripples of the d- and q-axes as Table 2. The multi-step MPCC method reduces the d-axis and q-axis current ripples by approximately 26.7 and 30.4 percent, respectively.

Figure 14 displays current ripples at various MPCC speeds without load. In Fig. 14, the multi-step MPCC method has less current ripples than the typical MPCC strategy. Thus, the multi-step MPCC method outperforms the classic MPCC strategy.

Traditional and multi-step MPCC techniques with a rated load of 1000r/min are shown in Figure 15. This strategy's current THD at 1000r/min is 8.39 percent. Its current THD at 1000r/min is 6.07 percent. Compared to the typical MPCC technique, the proposed strategy has lower THD and improved steady-state performance.

Fig. 16 shows the cost function experimental waveforms of the classic MPCC and multi-step MPCC techniques at 500r/min with no load. According to Eq. (10), the cost function is the difference between the predicted and reference currents. In Fig. 16, g is much smaller than index in the multi-step I MPCC method. That is, the multi-step MPCC strategy's predictive current is closer to the reference than the typical MPCC strategy's. Thus, the multi-step MPCC technique has improved SPMSM control performance.

3.4 Switching frequency of experimental results

Figure 17 displays the switching frequency waveforms of the traditional MPCC and multi-step MPCC techniques at 1000r/min with no load. An oscilloscope collects 125,016 sets of experimental data to directly evaluate the two techniques' switching frequency. Both strategies use 10 kHz sampling. Table 3 shows the switching frequency. The switching frequency of the two techniques is similar when the sample frequency is similar.

The aforementioned simulation and experimental results show that the standard MPCC and multistep MPCC techniques respond quickly to changes in SPMSM speed and torque. The current ripple of the multi-step MPCC approach is always less than the classic MPCC method at the same reference speed, indicating greater steady-state performance. The multi-step MPCC technique increased steady-state performance without increasing switching frequency. The multi-step technique's selected voltage vector is ideal in two control periods, thus the predictive current tracks the reference more accurately than the standard strategy. The above simulation and experimental results support the earlier theoretical study.

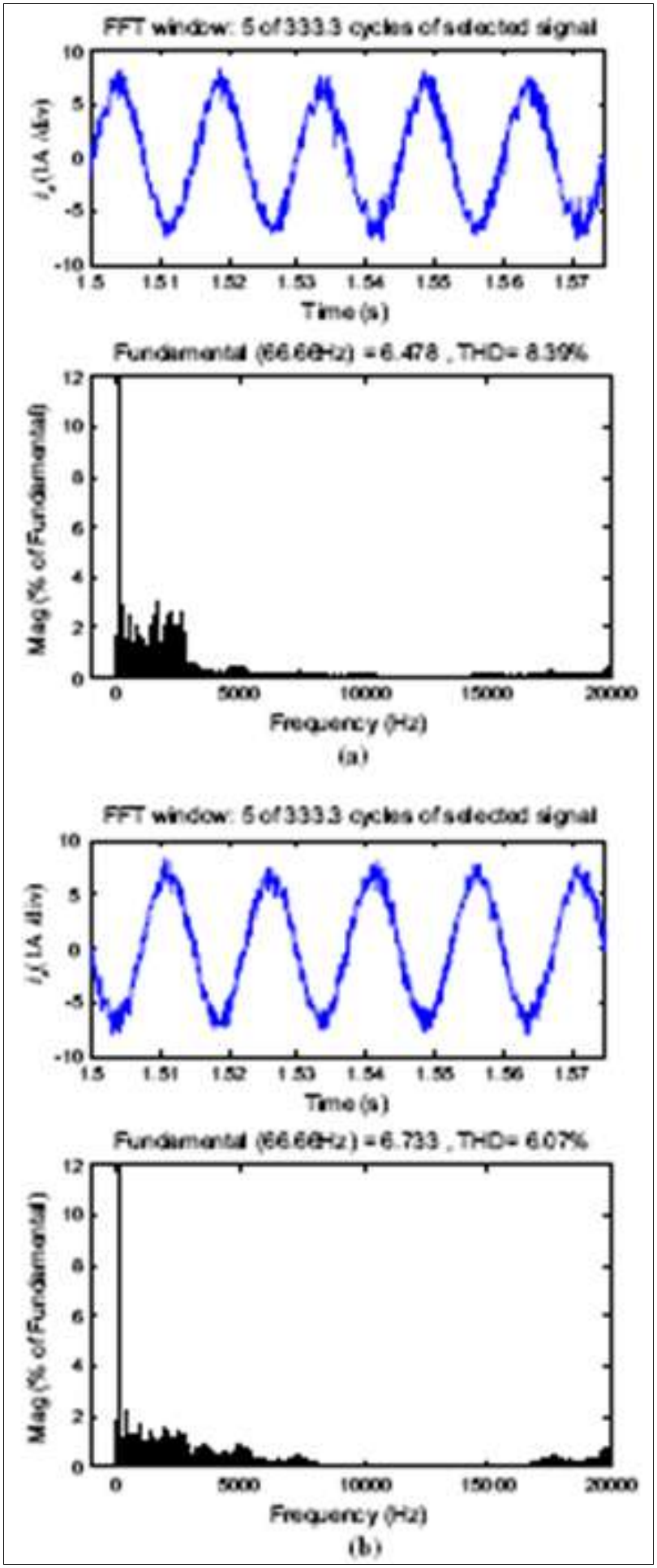

Fig 15: Steady-state performance experimental results at 1000r/min with the rated load: a traditional MPCC; b multi-step MPCC

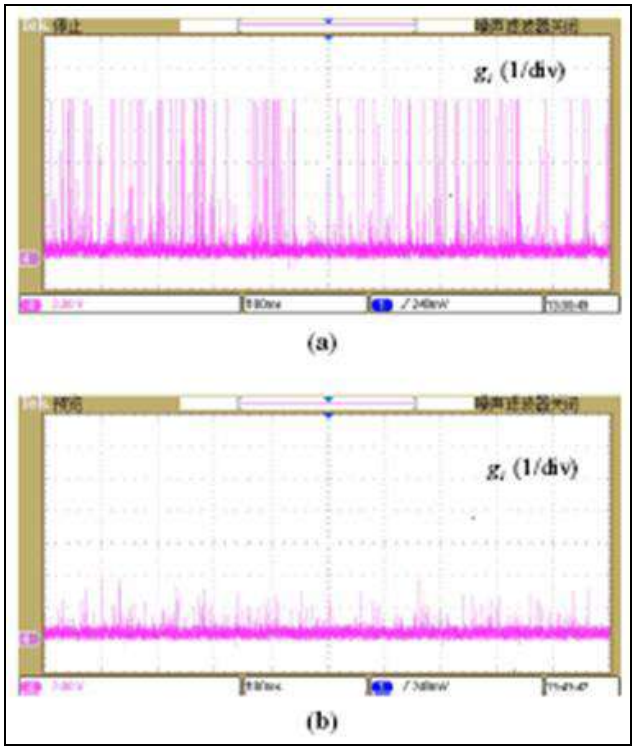

Fig 16: Cost function experimental waveforms at 500r/min without a load: a traditional MPCC; b multi-step MPCC

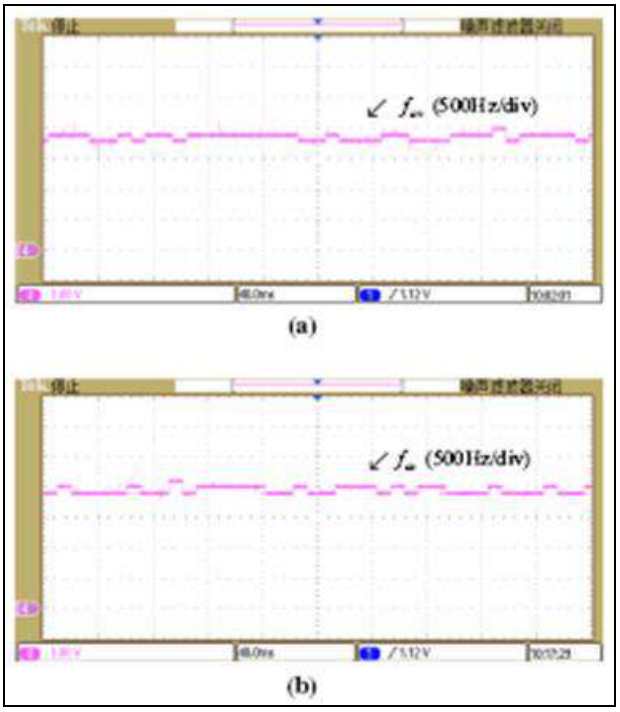

Fig 17: Experimental results of the switching frequency of the: a traditional MPCC; b multi-step MPCC

Table 3: Switching frequency of two control strategies at the same sampling frequency

Strategy	f_{av} (kHz)
The traditional MPCC	1.91
The multi-step MPCC	1.97

4. Conclusions

This research suggests a multi-step MPCC approach to decrease the present SPMSM ripple. The multi-step MPCC technique examines both the optimal and suboptimal voltage vectors. A voltage vector's optimality is also determined in two control periods. The experimental results in this research lead to the following conclusions. In terms of dynamic performance, the proposed and traditional MPCC strategies are identical. The current ripple of the multi-step MPCC approach is minimized in a wide speed range compared to the classic MPCC technique. In terms of switching frequency, the proposed solution matches the traditional MPCC strategy.

References

1. Petrov I, Niemelä M, Ponomarev P, Pyrhönen J. Rotor surface ferrite permanent magnets in electrical machines: advantages and limitations. IEEE Trans. Ind. Electron 2017;64(7):5314-5322.
2. Wang W, Zhang J, Cheng M. Common model predictive control for permanent-magnet synchronous machine drives considering single-phase open-circuit fault. IEEE Trans. Power Electron 2017;32(7):5862–5872.
3. Kim S, Park S, Kwak S. Simplified model predictive control method for three-phase four-leg voltage source inverters. J Power Electron 2016;16(6):2231-2242.
4. Vafaie MH, Dehkordi BM. Approach for classifying direct PCs applied to AC motor drives. IET Electric Power Appl 2019;13(3):385-401.
5. Vazquez S, Rodriguez J, Rivera M, Franquelo LG, Noram-buena M. Model predictive control for power converters and drives: advances and trends. IEEE Trans. Ind. Electron 2017;64(2):935-947.
6. Karamanakos P, Geyer T, Aguilera RP. Long-horizon direct model predictive control: modified sphere decoding for transient operation. IEEE Trans. Ind. Appl 2018;54(6):6060-6070.
7. Zhang Y, Xu D, Huang L. Generalized multiple-vector-based model predictive control for PMSM drives. IEEE Trans. Ind. Electron 2018;65(12):9356-9366.
8. Aguilera RP, Lezana P, Quevedo DE. Finite-control-set model predictive control with improved steady-state performance. IEEE Trans. Ind. Inform 2013;9(2):658-667.
9. Jin T, Shen X, Su T, Flesch R. Model predictive voltage control based on finite control set with computation time delay compensation for PV systems. IEEE Trans. Energy Convers 2019;34(1):330-338.
10. Zhang YC, Yang HT. Two-vector-based model predictive torque control without weighting factors for induction motor drives. IEEE Trans. Power Electron 2016;31(2):1381-1390.
11. Wang XH, Sun D. Three-vector-based low-complexity model predictive direct power control strategy for doubly fed induction generators. IEEE Trans. Power Electron 2017;32(1):773-782.
12. Siami M, Khaburi DA. Torque ripple reduction of predictive torque control for PMSM drives with parameter mismatch. IEEE Trans. Ind. Electron 2017;32(9):7160-7168.
13. Karamanakos P, Geyer T, Manias S. Direct voltage control of DC-DC boost converters using enumeration-based model predictive control. IEEE Trans. Power Electron 2014;29(2):968-978.
14. Ayad A, Karamanakos P. Direct model predictive current control strategy of quasi-Z-source inverters. IEEE Trans. Power Electron 2017’32(7):5786-5801.

15. Geyer T, Quevedo DE. Performance of multistep finite control set model predictive control for power electronics. IEEE Trans. Power Electron 2015;30(3):1633-1644.